PERGAMON

International Journal of Solids and Structures 37 (2000) 7259–7280

INTERNATIONAL JOURNAL OF SOLIDS and STRUCTURES

www.elsevier.com/locate/ijsolstr

Failure analysis of elasto-plastic material models on different levels of observation

Ellen Kuhl [a], Ekkehard Ramm [a], Kaspar Willam [b,*]

[a] *Institute of Structural Mechanics, University of Stuttgart, Pfaffenwaldring 7, D-70550 Stuttgart, Germany*

[b] *Department of Civil, Environmental and Architectural Engineering – CEAE Department, University of Colorado at Boulder, Campus Box 428, Boulder, CO 80309-0428, USA*

Received 6 October 1999; in revised form 23 January 2000

Abstract

This paper aims at characteristic failure mechanisms of cohesive frictional materials at two levels of observation: (a) at the macroscale of continuum elastoplasticity, and (b) at the microscale of active microplanes with arbitrary orientation. Thereby, the criteria for the loss of uniqueness and the loss of ellipticity will be discussed for a macroscopic as well as a microplane-based anisotropic plasticity formulation. In addition, conditions for shear dilatancy will be developed at the two scales which illustrate the necessity to couple normal and shear components at each microplane. © 2000 Elsevier Science Ltd. All rights reserved.

Keywords: Elastoplastic failure analysis; Microplane level; Extended Drucker–Prager model

1. Introduction

The prediction of failure caused by the deterioration of material properties is of great interest not only for material scientists but also for various practical engineering applications. Especially, the behavior of cohesive frictional materials like soils, concrete or rock which exhibit an entirely different response at increasing levels of confinement, is not yet fully understood and thus cannot be simulated properly. In contrast to metals, cohesive-frictional materials are characterized by a large contrast of tensile and compressive strength values due to strong pressure sensitivity. Consequently, their possible failure modes cover the wide range from purely decohesive failure in tension to ductile sliding failure in shear and compression. Moreover, the granular action of the aggregate causes frictional effects, which induce dilatational deformation as pointed out already by Reynolds (1885) as early as 1885. The suppression of shear dilatancy and concomitant confinement leads to ductile failure modes of the shear-compression type even in shear dominated loading situations.

Material deterioration usually starts at the microscopic level manifesting itself in the formation of microdefects such as microcracks or microvoids. Under progressive loading, the coalescence of these

* Corresponding author. Fax: +1-303-492-7317.

E-mail address: willam@bechtel.colorado.edu (K. Willam).

0020-7683/00/$ - see front matter
PII: S0020-7683(00)00198-0

microdefects results in the development of macroscopic failure zones in the form of shear bands or macroscopic cracks while the rest of the structure might even exhibit unloading. Especially for cohesive frictional materials, the phenomenon of strain localization induces a highly anisotropic material response. Since the resulting zones of localized deformation can be understood as precursors to structural failure, the appropriate prediction of strain localization is of great importance.

These characteristic properties of cohesive frictional materials are normally captured within the framework of the theory of plasticity. The classical two invariant plasticity formulation of Drucker and Prager (1952) was one of the first models which take into account the above mentioned phenomena. Within this study, we will extend the original Drucker–Prager formulation in the form of a parabola in the two invariant space. The two parameters, the friction coefficient and the cohesive yield strength, can be directly related to the uniaxial tensile and compressive strength determined from experimental measurements.

The performance of the parabolic two invariant plasticity formulation will be investigated by means of a systematic study of diffuse and localized failure. Traditionally, different stages of material failure can be distinguished. While the loss of uniqueness of the incremental response corresponds to a singularity of the elasto-plastic tangent operator, the singular behavior of the elasto-plastic acoustic tensor signals a change of the type of the governing partial differential equations which manifests itself in the formation of a spatial discontinuity in the strain rate field (Thomas, 1961 or Hill, 1958, 1962). For geomaterials, particularly the latter condition is of interest, since it often develops in the hardening regime when non–associated plasticity is used (Rudnicki and Rice, 1975). This localization condition attains a geometrical interpretation in the plane of the Mohr stress coordinates (Mohr, 1882). By imposing tangency between the largest stress circle and the localization condition which takes the form of an ellipse, the critical failure angle as well as the critical hardening modulus may be determined (Benallal, 1992; Benallal and Comi, 1996; Iordache and Willam, 1998, 1997).

The development of localized failure is an extremely anisotropic process. The two invariant Drucker–Prager formulation, however, is isotropic to start with and captures failure only indirectly in the form of a singularity of the acoustic tensor which reflects the stress induced anisotropy of the tangent operator. The microplane concept is one of the classical concepts to describe anisotropy based on the idea of formulating constitutive relations by integrating the planewise material behavior over all possible directions in space. Obviously, the advantage of this idea, which originally dates back to Mohr (1900a,b), is that material anisotropy is taken into account in a natural and very simple way. Nevertheless, the original microplane models of Bažant and Gambarova (1984), Bažant and Prat (1988) and Carol et al. (1992) were developed exclusively for elasto-damaging materials. The concept of formulating material behavior in a planewise sense has become well accepted when modeling sliding in crystallographic metals, a phenomenon, which is independent of the state of hydrostatic pressure. However, to model the failure of cohesive frictional materials, a pressure-sensitive microplane-based plasticity model has to be introduced. Thereby, the two invariants of the Drucker–Prager plasticity model, namely, the trace of the stress tensor and the second invariant of the stress deviator, will be replaced by the plane based volumetric and tangential stress component, respectively. For each direction, an individual yield function in terms of these two components determines the amount of plastic flow. Consequently, any type of anisotropic material behavior can be described in a natural fashion since the macroscopic stress tensor is given as the integral of the resulting planewise stress components of all possible directions in space.

The objective of this paper is the comparison of the failure characteristics of a well-known macroscopic plasticity formulation with those of a microplane-based plasticity model. The paper is organized as follows. After briefly summarizing the set of constitutive equations for the standard macroscopic plasticity model, a short introduction into failure analysis will be given. The theoretical background will be illustrated by means of localization analysis of the simple shear problem using non-associated parabolic Drucker–Prager plasticity. It will be shown, how the localization condition may be interpreted geometrically in the plane of Mohr's coordinates. The simple shear problem will be used in order to study the features of the model

under moderate and high confinement. In the second part of the paper, a microplane-based plasticity model will be discussed which is closely related to the macroscopic parabolic Drucker–Prager model. Special attention will be given to the conditions of pressure-sensitivity to capture the Reynolds effect and the relation between the microplane parameters and the macroscopic material properties. Again, the behavior of the model will be illustrated by means of the model problem of simple shear. We will conclude by pointing out the basic similarities and conceptual differences between the microplane-based and the macroscopic plasticity model.

2. Macroscopic elasto-plasticity

We start by briefly summarizing the well-known set of equations of a macroscopic elasto-plasticity model which is herein restricted to the small strain setting. Consequently, the strain tensor $\boldsymbol{\epsilon} = \nabla^{\mathrm{sym}}\boldsymbol{u}$, is the symmetric part of the displacement gradient, which can be additively decomposed into an elastic and a plastic part:

$$\boldsymbol{\epsilon} = \boldsymbol{\epsilon}^{\mathrm{el}} + \boldsymbol{\epsilon}^{\mathrm{pl}}. \tag{1}$$

Moreover, a free energy Ψ^{mac} is introduced in terms of the total strains, the plastic strains and an internal variable κ which accounts for the hardening behavior:

$$\Psi^{\mathrm{mac}} = \Psi^{\mathrm{mac}}(\boldsymbol{\epsilon}, \boldsymbol{\epsilon}^{\mathrm{pl}}, \kappa) = \frac{1}{2}\,\boldsymbol{\epsilon}^{\mathrm{el}} : \mathscr{E}^{\mathrm{el}} : \boldsymbol{\epsilon}^{\mathrm{el}} + \int_0^{\kappa} Y_F^{\mathrm{mac}}(\kappa)\,\mathrm{d}\hat{\kappa}. \tag{2}$$

With the classical arguments, the evaluation of the Clausius–Duhem inequality yields the stress tensor $\boldsymbol{\sigma}$ as thermodynamically conjugate variable to the plastic strain rate with

$$\boldsymbol{\sigma} = \frac{\partial \Psi^{\mathrm{mac}}}{\partial \boldsymbol{\epsilon}^{\mathrm{el}}} \quad \text{and} \quad \dot{\boldsymbol{\sigma}} = \mathscr{E}^{\mathrm{el}} : \left[\dot{\boldsymbol{\epsilon}} - \dot{\boldsymbol{\epsilon}}^{\mathrm{pl}}\right], \tag{3}$$

whereby the relation between the stress rates and the elastic strain rates is defined in terms of the fourth order elasticity tensor $\mathscr{E}^{\mathrm{el}}$. Furthermore, the yield stress Y_F^{mac} can be obtained as conjugate variable to the internal variable κ, with

$$Y_F^{\mathrm{mac}} = \frac{\partial \Psi^{\mathrm{mac}}}{\partial \kappa} \quad \text{and} \quad \dot{Y}_F^{\mathrm{mac}} = H\dot{\kappa} \tag{4}$$

such that the relation between the rate of the yield stress and the internal variable defines the hardening modulus H. The yield function F^{mac}

$$F^{\mathrm{mac}}\left(\boldsymbol{\sigma}, Y_F^{\mathrm{mac}}\right) \leqslant 0 \quad \text{with } \boldsymbol{v} := \frac{\partial F^{\mathrm{mac}}}{\partial \boldsymbol{\sigma}} \tag{5}$$

characterizes the elastic domain. Its normal in the stress space will be denoted by $\boldsymbol{v}$. The evolution of plastic strains is governed by the plastic flow rule

$$\dot{\boldsymbol{\epsilon}}^{\mathrm{pl}} = \dot{\gamma}\,\boldsymbol{\mu} \quad \text{with } \boldsymbol{\mu} := \frac{\partial Q^{\mathrm{mac}}}{\partial \boldsymbol{\sigma}}, \tag{6}$$

whereby $\boldsymbol{\mu}$ denotes the normal to the plastic potential Q^{mac} which differs from the yield function F^{mac} in the general non-associated case. The set of constitutive equations is completed by the Kuhn-Tucker conditions

$$F^{\mathrm{mac}} \leqslant 0, \;\; \dot{\gamma} \geqslant 0, \;\; F^{\mathrm{mac}}\dot{\gamma} = 0 \tag{7}$$

and the consistency condition

$$\dot{F}^{\mathrm{mac}}\dot{\gamma} = 0. \tag{8}$$

The latter defines the plastic multiplier γ

$$\dot{\gamma} = \frac{1}{h}\, \boldsymbol{\nu} : \boldsymbol{\mathcal{E}}^{\mathrm{el}} : \dot{\boldsymbol{\epsilon}} \tag{9}$$

with $h = H + \boldsymbol{\nu} : \boldsymbol{\mathcal{E}}^{\mathrm{el}} : \boldsymbol{\mu}$. Finally, the elasto-plastic tangent operator $\boldsymbol{\mathcal{E}}^{\mathrm{ep}}$ relating the stress and strain rates takes the classical form of a rank-one update of the elastic material operator $\boldsymbol{\mathcal{E}}^{\mathrm{el}}$, such that

$$\dot{\boldsymbol{\sigma}} = \boldsymbol{\mathcal{E}}^{\mathrm{ep}} : \dot{\boldsymbol{\epsilon}} \quad \text{with } \boldsymbol{\mathcal{E}}^{\mathrm{ep}} = \frac{\partial \boldsymbol{\sigma}}{\partial \boldsymbol{\epsilon}} = \boldsymbol{\mathcal{E}}^{\mathrm{el}} - \frac{1}{h}\, \boldsymbol{\mathcal{E}}^{\mathrm{el}} : \boldsymbol{\mu} \otimes \boldsymbol{\nu} : \boldsymbol{\mathcal{E}}^{\mathrm{el}}. \tag{10}$$

3. Macroscopic failure analysis

This section introduces different criteria to indicate the onset of failure. As depicted in Fig. 1, increased loading leads to a progression of kinematic deterioration which starts from diffuse failure, and which progresses through localized failure to a discrete failure pattern. Thereby, diffuse failure will be referred to as a loss of uniqueness in the spirit of an algebraic singularity. The following discussion will be restricted to the first two stages of failure, diffuse failure characterized through the loss of uniqueness and localized failure indicated through the loss of ellipticity.

3.1. Diffuse failure–loss of uniqueness

According to Fig. 1, diffuse failure maintains continuity in the rates of displacement and displacement gradient fields. It corresponds to a stationary stress state indicated through the limit point condition

$$\dot{\boldsymbol{\sigma}} = \boldsymbol{0}. \tag{11}$$

For incrementally linear elasto-plastic materials with $\dot{\boldsymbol{\sigma}} = \boldsymbol{\mathcal{E}}^{\mathrm{ep}} : \dot{\boldsymbol{\epsilon}}$, such that

$$\boldsymbol{\mathcal{E}}^{\mathrm{ep}} : \dot{\boldsymbol{\epsilon}} = \boldsymbol{0}, \tag{12}$$

the condition for the loss of uniqueness is equivalent to a singular behavior of the elasto-plastic tangent operator $\boldsymbol{\mathcal{E}}^{\mathrm{ep}}$,

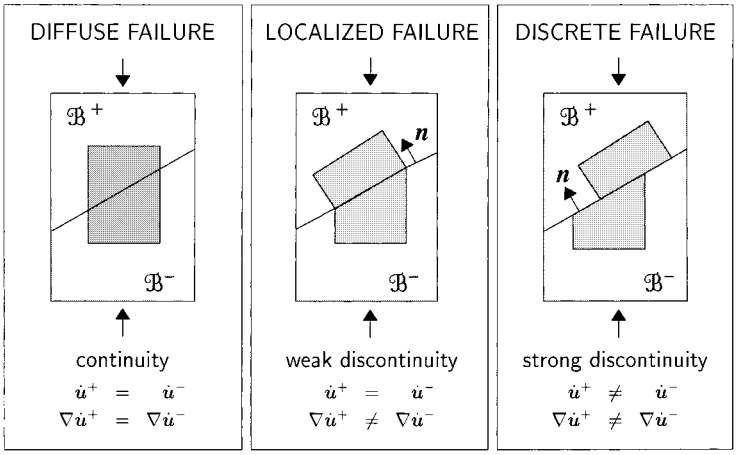

Fig. 1. Schematic representation of progressive kinematic degradation.

$$\det \boldsymbol{\mathscr{E}}^{\mathrm{ep}} \stackrel{!}{=} 0 \quad \text{with } \boldsymbol{\mathscr{E}}^{\mathrm{ep}} = \boldsymbol{\mathscr{E}}^{\mathrm{el}} - \frac{\overline{\boldsymbol{\mu}} \otimes \overline{\boldsymbol{v}}}{h}. \tag{13}$$

Note, that this tangent operator can be expressed as a rank one update of the elastic material operator $\boldsymbol{\mathscr{E}}^{\mathrm{el}}$, whereby the update tensors $\overline{\boldsymbol{\mu}}$ and $\overline{\boldsymbol{v}}$ take the following form:

$$\begin{aligned} \overline{\boldsymbol{\mu}} &:= \boldsymbol{\mathscr{E}}^{\mathrm{el}} : \boldsymbol{\mu}, \\ \overline{\boldsymbol{v}} &:= \boldsymbol{v} : \boldsymbol{\mathscr{E}}^{\mathrm{el}}. \end{aligned} \tag{14}$$

Instead of solving the eigenvalue problem arising from Eq. (13), the following generalized eigenvalue problem $\det[[\boldsymbol{\mathscr{E}}^{\mathrm{el}}]^{-1} : \boldsymbol{\mathscr{E}}^{\mathrm{ep}}] \stackrel{!}{=} 0$ is solved. Preconditioning of the elasto-plastic tangent operator with the inverse elasticity tensor yields the following relation:

$$\left[\boldsymbol{\mathscr{E}}^{\mathrm{el}}\right]^{-1} : \boldsymbol{\mathscr{E}}^{\mathrm{ep}} = \boldsymbol{\mathscr{I}} - \left[\boldsymbol{\mathscr{E}}^{\mathrm{el}}\right]^{-1} : \frac{\overline{\boldsymbol{\mu}} \otimes \overline{\boldsymbol{v}}}{h}, \tag{15}$$

whereby $\boldsymbol{\mathscr{I}}$ denotes the fourth order unit tensor with the components $[\boldsymbol{\mathscr{I}}]_{ijkl} = (\delta_{ik}\,\delta_{jl})^{\mathrm{sym}}$. Due to the rank-one update structure of the elasto-plastic tangent operator, the critical eigenvalue $\lambda_{\min}$ of the generalized eigenvalue problem can be evaluated in closed form. This motivates the introduction of the scalar-valued measure of material integrity $D_{\mathscr{E}}$,

$$\lambda_{\min}\left[\left[\boldsymbol{\mathscr{E}}^{\mathrm{el}}\right]^{-1} : \boldsymbol{\mathscr{E}}^{\mathrm{ep}}\right] = 1 - D_{\mathscr{E}} \quad \text{with } D_{\mathscr{E}} := \frac{\boldsymbol{v} : \left[\boldsymbol{\mathscr{E}}^{\mathrm{el}}\right]^{-1} : \boldsymbol{\mu}}{\boldsymbol{v} : \boldsymbol{\mathscr{E}}^{\mathrm{el}} : \boldsymbol{\mu} + H}. \tag{16}$$

From the above definition, the following necessary condition for the loss of uniqueness and the critical hardening modulus for the loss of uniqueness H may be determined.

$$1 - D_{\mathscr{E}} \stackrel{!}{=} 0 \quad \rightarrow \quad H = 0. \tag{17}$$

Note, that the criterion presented above can only be understood as a necessary condition for the loss of uniqueness. For non-symmetric elasto-plastic tangent operators arising from non-associated plasticity formulations, however, the vanishing determinant of the symmetric part of the tangent operator, $\det[\boldsymbol{\mathscr{E}}^{\mathrm{ep}}]^{\mathrm{sym}} \stackrel{!}{=} 0$, provides a more critical lower bound condition according to the Bromwich bounds. Consequently, for materials with non-symmetric material operators, loss of stability synonymous with a singularity of the symmetric tangent operator takes place before the limit point condition (11) is reached. In this case, the critical hardening modulus may still be positive.

3.2. Localized failure–loss of ellipticity

The localization condition derived in the following is based on the early works of Hadamard (1903), Thomas (1961) and Hill (1958, 1962). In contrast to the diffuse failure mode described in the previous section, localized failure of weak discontinuities is characterized through a discontinuity in the rate of the displacement gradient while the field of the displacement rate itself is still continuous. According to Maxwell's compatibility condition, the jump in the rate of the displacement gradient may be expressed exclusively in terms of a scalar-valued jump amplitude ξ, the unit jump vector $\boldsymbol{m}$ and the unit normal vector to the discontinuity surface $\boldsymbol{n}$:

$$\left[\left|\nabla \dot{\boldsymbol{u}}\right|\right] = \xi\, \boldsymbol{m} \otimes \boldsymbol{n} \quad \rightarrow \quad [|\dot{\boldsymbol{\epsilon}}|] = \xi\, [\, \boldsymbol{m} \otimes \boldsymbol{n}\,]^{\mathrm{sym}}. \tag{18}$$

Equilibrium along the discontinuity surface according to Cauchy's lemma requires that

$$\left[\left|\dot{\boldsymbol{t}}\right|\right] := \dot{\boldsymbol{t}}^{+} - \dot{\boldsymbol{t}}^{-} = \boldsymbol{0}, \tag{19}$$

whereby the traction vector $\boldsymbol{t} = \boldsymbol{n} \cdot \boldsymbol{\sigma}$ is defined according to Cauchy's theorem, such that

$$\left[|\dot{\boldsymbol{t}}|\right] = \boldsymbol{n} \cdot \left[|\dot{\boldsymbol{\sigma}}|\right] = \boldsymbol{n} \cdot \left[|\mathscr{E}^{\mathrm{ep}} : \dot{\boldsymbol{\epsilon}}|\right] = \boldsymbol{0}. \tag{20}$$

With the assumption of a linear comparison solid, $[|\mathscr{E}^{\mathrm{ep}}|] := \mathscr{E}^{\mathrm{ep}+} - \mathscr{E}^{\mathrm{ep}-} = \boldsymbol{0}$, as proposed by Hill (1958), the localization condition may be expressed in the following form:

$$\xi\, \boldsymbol{q}^{\mathrm{ep}} \cdot \boldsymbol{m} = 0 \quad \text{with } \boldsymbol{q}^{\mathrm{ep}} := \boldsymbol{n} \cdot \mathscr{E}^{\mathrm{ep}} \cdot \boldsymbol{n}, \tag{21}$$

whereby $\boldsymbol{q}^{\mathrm{ep}}$ denotes the elasto-plastic acoustic tensor. The necessary condition for the onset of localization indicating the loss of ellipticity is thus characterized through the singularity of this acoustic tensor.

$$\det \boldsymbol{q}^{\mathrm{ep}} \overset{!}{=} 0 \quad \text{with } \boldsymbol{q}^{\mathrm{ep}} = \boldsymbol{q}^{\mathrm{el}} - \frac{\boldsymbol{e}_\mu \otimes \boldsymbol{e}_v}{h}. \tag{22}$$

Note, that this elasto-plastic acoustic tensor can be expressed as a rank-one update of the elastic acoustic tensor $\boldsymbol{q}^{\mathrm{el}} = \boldsymbol{n} \cdot \mathscr{E}^{\mathrm{el}} \cdot \boldsymbol{n}$, whereby we have introduced the following abbreviations for the update vectors $\boldsymbol{e}_\mu$ and $\boldsymbol{e}_v$:

$$\begin{aligned} \boldsymbol{e}_\mu &:= \boldsymbol{n} \cdot \mathscr{E}^{\mathrm{el}} : \boldsymbol{\mu}, \\ \boldsymbol{e}_v &:= \boldsymbol{v} : \mathscr{E}^{\mathrm{el}} \cdot \boldsymbol{n}. \end{aligned} \tag{23}$$

Again, instead of solving the original eigenvalue problem (22), the generalized eigenvalue problem $\det[[\boldsymbol{q}^{\mathrm{el}}]^{-1} \cdot \boldsymbol{q}^{\mathrm{ep}}] \overset{!}{=} 0$ is used to identify the singularity (Ottosen and Runesson, 1991). Therefore, pre-conditioning of the elasto-plastic acoustic tensor with the inverse of the elastic acoustic tensor leads to

$$\left[\boldsymbol{q}^{\mathrm{el}}\right]^{-1} \cdot \boldsymbol{q}^{\mathrm{ep}} = \boldsymbol{1} - \left[\boldsymbol{q}^{\mathrm{el}}\right]^{-1} \cdot \frac{\boldsymbol{e}_\mu \otimes \boldsymbol{e}_v}{h} \tag{24}$$

with $\boldsymbol{1}$ denoting the second order unit tensor with components $[\boldsymbol{1}]_{ij} = \delta_{ij}$. The closed form solution for the critical eigenvalue $\lambda_{\min}$ motivates the introduction of the scalar-valued measure of localization integrity D_q.

$$\lambda_{\min}\left[\left[\boldsymbol{q}^{\mathrm{el}}\right]^{-1} \cdot \boldsymbol{q}^{\mathrm{ep}}\right] = 1 - D_q \quad \text{with } D_q := \frac{\boldsymbol{e}_v \cdot \left[\boldsymbol{q}^{\mathrm{el}}\right]^{-1} \cdot \boldsymbol{e}_\mu}{\boldsymbol{v} : \mathscr{E}^{\mathrm{el}} : \boldsymbol{\mu} + H}. \tag{25}$$

It defines a necessary condition for localization as well as the critical hardening modulus H indicating the loss of ellipticity:

$$1 - D_q \overset{!}{=} 0 \quad \rightarrow \quad H = \boldsymbol{e}_v \cdot \left[\boldsymbol{q}^{\mathrm{el}}\right]^{-1} \cdot \boldsymbol{e}_\mu - \boldsymbol{v} : \mathscr{E}^{\mathrm{el}} : \boldsymbol{\mu}. \tag{26}$$

4. Example: non-associated Drucker–Prager plasticity

4.1. Specification of yield function and plastic potential

In order to characterize the elasto-plastic material model, the yield function F^{mac} and the plastic potential Q^{mac} must be specified. Herein, we will restrict ourselves to formulations depending on the first invariant of the stress tensor I_1 and the second invariant of the stress deviator J_2 with

$$\begin{aligned} I_1 &= \boldsymbol{\sigma} : \boldsymbol{1}, \\ J_2 &= \tfrac{1}{2}\boldsymbol{\sigma}^{\mathrm{dev}} : \boldsymbol{\sigma}^{\mathrm{dev}}, \end{aligned} \tag{27}$$

whereby the deviator of the stress tensor is defined as $\boldsymbol{\sigma}^{\mathrm{dev}} := \boldsymbol{\sigma} - \frac{1}{3}[\boldsymbol{\sigma} : \boldsymbol{1}]\, \boldsymbol{1}$. The two-invariant formulation in terms of I_1 and J_2 was originally introduced by Drucker and Prager (1952) in order to model the plastic

behavior of soils. A generalization of the original two parameter model which was characterized exclusively in terms of the friction angle α_F^{mac} and the yield stress Y_F^{mac} may be expressed in the following form:

$$F^{\text{mac}} = F^{\text{mac}}(I_1, J_2, Y_F^{\text{mac}}) = J_2^m - z\left[c\,\alpha_F^{\text{mac}}\,I_1 - Y_F^{\text{mac}}\right]^n. \tag{28}$$

Its dependence on four additional parameters enables the representation of a linear, an elliptic, a hyperbolic and a parabolic shape in the $\{I_1, \sqrt{J_2}\}$-space (see Liebe and Willam (1999) for details). Herein, we will apply a parabolic version of the generalized formulation, which results from choosing $m = 1$, $z = -1$, $c = 1$ and $n = 1$, such that

$$F^{\text{mac}} = F^{\text{mac}}(I_1, J_2, Y_F^{\text{mac}}) = J_2 + \alpha_F^{\text{mac}}\,I_1 - Y_F^{\text{mac}}. \tag{29}$$

The remaining two Drucker–Prager parameters can be derived uniquely from uniaxial tension and compression tests (compare Fig. 2). They can thus be expressed in terms of the tensile and compressive strength values f_{t} and f_{c} as

$$\alpha_F^{\text{mac}} = \frac{f_{\text{c}} - f_{\text{t}}}{3} \quad \text{and} \quad Y_F^{\text{mac}} = \frac{f_{\text{c}}\,f_{\text{t}}}{3}. \tag{30}$$

In the following, we will assume a non-associated plasticity formulation for which the plastic potential Q^{mac} is chosen independently from the yield function F^{mac}:

$$Q^{\text{mac}} = Q^{\text{mac}}(I_1, J_2, Y_Q^{\text{mac}}) = J_2 + \alpha_Q^{\text{mac}}\,I_1 - Y_Q^{\text{mac}}. \tag{31}$$

It is thus characterized through the two additional parameters α_Q^{mac} and Y_Q^{mac}. Consequently, the normal to the yield surface $\boldsymbol{\nu}$ and the normal to the plastic potential $\boldsymbol{\mu}$ take the following form:

$$\begin{aligned} \boldsymbol{\nu} &= \frac{\partial F^{\text{mac}}}{\partial \boldsymbol{\sigma}} = \boldsymbol{\sigma}^{\text{dev}} + \alpha_F^{\text{mac}}\,\mathbf{1}, \\ \boldsymbol{\mu} &= \frac{\partial Q^{\text{mac}}}{\partial \boldsymbol{\sigma}} = \boldsymbol{\sigma}^{\text{dev}} + \alpha_Q^{\text{mac}}\,\mathbf{1}. \end{aligned} \tag{32}$$

Moreover, the explicit forms of the abbreviations $\boldsymbol{e}_\nu$ and $\boldsymbol{e}_\mu$ introduced in Eq. (23), together with the definition of the fourth order elasticity tensor

$$\mathfrak{E}^{\text{el}} = \frac{E\,\nu}{[1+\nu][1-2\nu]}\,\mathbf{1}\otimes\mathbf{1} + \frac{E}{1+\nu}\,\mathfrak{I} \tag{33}$$

result in the following expressions:

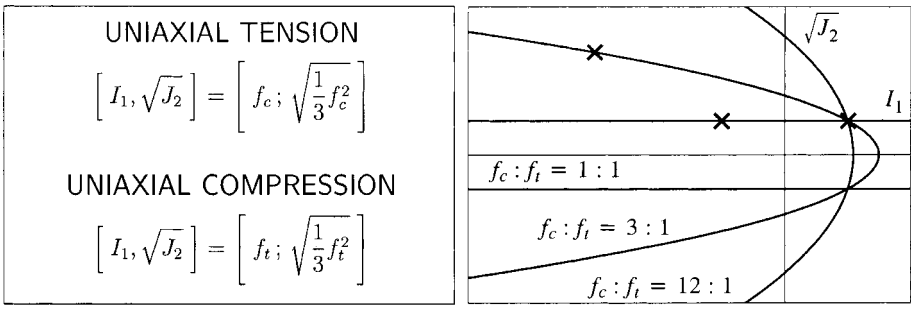

Fig. 2. Parabolic Drucker–Prager yield function.

$$\begin{aligned} \boldsymbol{e}_v &= \boldsymbol{v} : \mathscr{E}^{\mathrm{el}} \cdot \boldsymbol{n} = \frac{E}{1+v}\, \boldsymbol{\sigma}^{\mathrm{dev}} \cdot \boldsymbol{n} + \frac{E}{1-2v}\, \alpha_F^{\mathrm{mac}}\, \boldsymbol{n}, \\ \boldsymbol{e}_\mu &= \boldsymbol{n} \cdot \mathscr{E}^{\mathrm{el}} : \boldsymbol{\mu} = \frac{E}{1+v}\, \boldsymbol{\sigma}^{\mathrm{dev}} \cdot \boldsymbol{n} + \frac{E}{1-2v}\, \alpha_Q^{\mathrm{mac}}\, \boldsymbol{n}. \end{aligned} \tag{34}$$

4.2. Geometric interpretation of localization condition

This section provides a geometric illustration of the localization condition which can be interpreted as tangency condition between the largest Mohr circle of stress and the geometric representation of the localization condition. The latter will be shown to plot as an ellipse in the coordinates of Mohr. The geometric representation of failure criteria goes back to the early works of Mohr (1882, 1900a,b), who related material failure to the tangency between the stress circle and a failure surface. A reinterpretation in the sense of localized failure was given by Benallal (1992) and Benallal and Comi (1996) for elasto-plastic material models. Extensions to Cosserat-type material formulations and enhanced plasticity models have been presented only recently by Iordache and Willam (1998, 1997) and Liebe and Willam (1999). In a similar context, the localization of elasto-damaging materials was discussed by Pijaudier-Cabot and Benallal (1993) and Rizzi et al. (1995). In the following, we will briefly summarize the basic ideas of the geometric localization analysis for the general non-associated parabolic Drucker–Prager plasticity model introduced in the previous section. In Section 3.2, a condition which indicates the onset of localization has been derived. According to Eq. (26), it takes the following form:

$$H + \boldsymbol{v} : \mathscr{E}^{\mathrm{el}} : \boldsymbol{\mu} = \boldsymbol{e}_v \cdot \left[\boldsymbol{q}^{\mathrm{el}}\right]^{-1} \cdot \boldsymbol{e}_\mu. \tag{35}$$

Herein, $[\boldsymbol{q}^{\mathrm{el}}]^{-1}$ denotes the inverse of the elastic acoustic tensor, which can be determined analytically with the help of the Sherman–Morrison formula.

$$\left[\boldsymbol{q}^{\mathrm{el}}\right]^{-1} = \frac{2[1+v]}{E}\mathbf{1} - \frac{1+v}{E[1-v]}\boldsymbol{n} \otimes \boldsymbol{n}. \tag{36}$$

In the following, the localization condition (35) will be transformed into Mohr's coordinates σ_{N} and σ_{T} with

$$\begin{aligned} \sigma_{\mathrm{N}} &:= \boldsymbol{n} \cdot \boldsymbol{\sigma} \cdot \boldsymbol{n}, \\ \sigma_{\mathrm{T}}^2 &:= [\boldsymbol{\sigma} \cdot \boldsymbol{n}] \cdot [\boldsymbol{\sigma} \cdot \boldsymbol{n}] - \sigma_{\mathrm{N}}^2. \end{aligned} \tag{37}$$

A combination of Eq. (35) with Eqs. (32), (34) and (36) defines an ellipse in the plane of the Mohr stress coordinates. It can be expressed as follows:

$$\frac{[\sigma_{\mathrm{N}} - \sigma_{\mathrm{O}}]^2}{A^2} + \frac{\sigma_{\mathrm{T}}^2}{B^2} = 1 \tag{38}$$

with σ_{O} characterizing the center of the ellipse, while A and B determine its size in the normal and tangential direction, respectively.

$$\begin{aligned} \sigma_{\mathrm{O}} &= \frac{1}{3} I_1 - \frac{1+v}{2[1-2v]} \left[\alpha_F^{\mathrm{mac}} + \alpha_Q^{\mathrm{mac}}\right], \\ A^2 &= 2\, \frac{1-v}{1-2v}\, B^2, \\ B^2 &= \frac{1+v}{2E} H + J_2 + \frac{[1+v]^2}{8[1-2v][1-v]} \left[\alpha_F^{\mathrm{mac}} + \alpha_Q^{\mathrm{mac}}\right]^2 + \frac{1+v}{1-v}\, \alpha_F^{\mathrm{mac}}\, \alpha_Q^{\mathrm{mac}}. \end{aligned} \tag{39}$$

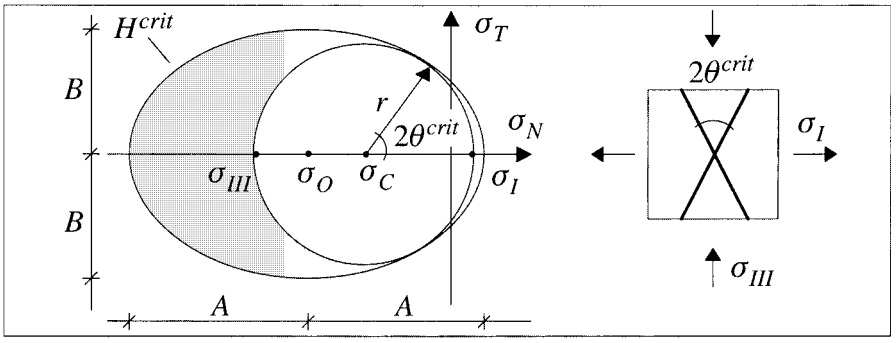

Fig. 3. Localization ellipse and major stress circle in the Mohr coordinates.

A typical localization ellipse is illustrated in Fig. 3. Note, that the center and the shape of the ellipse are not influenced by the hardening modulus H. The hardening modulus only influences the size of the corresponding ellipse. In addition to the localization ellipse, Fig. 3 depicts the Mohr circle of stress

$$[\sigma_{\mathrm{N}} - \sigma_{\mathrm{C}}]^2 + \sigma_{\mathrm{T}}^2 = r^2, \tag{40}$$

which characterizes the actual critical stress state. Herein, σ_{C} and r denote the center and the radius of the circle, respectively. They can be expressed in terms of the principal stresses σ_{I} and σ_{III}.

$$\begin{aligned} \sigma_{\mathrm{C}} &= \frac{\sigma_{\mathrm{I}} + \sigma_{\mathrm{III}}}{2}, \\ r &= \frac{\sigma_{\mathrm{I}} - \sigma_{\mathrm{III}}}{2}. \end{aligned} \tag{41}$$

The tangency condition between localization ellipse and the Mohr circle results in a quadratic equation defining the analytical solutions for critical failure angle Θ^{crit} and the critical hardening modulus H^{crit}. For the non-associated Drucker–Prager plasticity model according to Eq. (39), the critical failure angle may be expressed as follows:

$$\tan^2 \Theta^{\mathrm{crit}} = \frac{r - [1-2\nu][\sigma_{\mathrm{C}} - I_1/3] + [1+\nu]\left[\alpha_F^{\mathrm{mac}} + \alpha_Q^{\mathrm{mac}}\right]/2}{r + [1-2\nu][\sigma_{\mathrm{C}} - I_1/3] + [1+\nu]\left[\alpha_F^{\mathrm{mac}} + \alpha_Q^{\mathrm{mac}}\right]/2}. \tag{42}$$

Obviously, the critical failure angle is strongly influenced by the friction coefficient α_F^{mac} and the dilatancy parameter α_Q^{mac}. Furthermore, the failure angle is also influenced by Poisson's ratio ν. The analytical solution for the critical hardening modulus H^{crit} takes the following form:

$$\begin{aligned} H^{\mathrm{crit}} = \frac{2E}{1+\nu}\Bigg[& [1-2\nu]\left[\sigma_{\mathrm{C}} - \frac{1}{3}I_1 + \frac{1+\nu}{2[1-2\nu]}\left[\alpha_F^{\mathrm{mac}} + \alpha_Q^{\mathrm{mac}}\right]\right]^2 + r^2 - J_2 - \frac{[1+\nu]^2}{8[1-2\nu][1-\nu]} \\ & \times \left[\alpha_F^{\mathrm{mac}} + \alpha_Q^{\mathrm{mac}}\right]^2 - \frac{[1+\nu]}{[1-\nu]}\alpha_F^{\mathrm{mac}}\alpha_Q^{\mathrm{mac}}\Bigg]. \end{aligned} \tag{43}$$

4.3. Model problem of simple shear

In the following, the localization condition will be established for the model problem of simple shear. The simple shear test, which is realized experimentally through the shear box experiment, is a strain

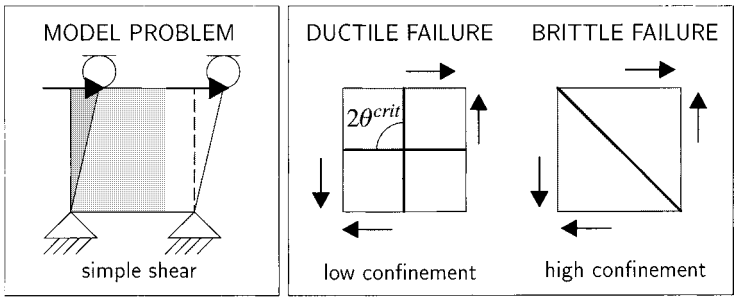

Fig. 4. Model problem – simple shear.

controlled test. When experimentally studied in a shear box experiment, nonlinear elastic, anisotropic elastic and pressure sensitive elasto-plastic materials exhibit a dilatant behavior. The phenomenon of dilatancy had been first established more than a hundred years ago by Reynolds (1885) and is thus often referred to as Reynolds effect. Due to the constitutive coupling of normal and shear components, the observed failure modes vary from a purely ductile shear failure to a compression failure of brittle nature, (compare Fig. 4). As a natural consequence of the Reynolds effect, an apparent hardening can be observed due to the confinement of dilatancy.

The question of shear dilatancy is directly related to the volumetric component of the flow rule (Willam et al., 1999). In fact, a sufficient condition for volumetric–deviatoric coupling may be formulated in terms of

$$\mathbf{1} : \mathscr{E}^{\mathrm{el}} : \boldsymbol{\mu} > 0 \quad \text{or} \quad \alpha_Q^{\mathrm{mac}} > 0 \tag{44}$$

to account for the Reynolds effect in continuum plasticity.

In a numerical simulation, all strain components except for the in-plane shear strain ϵ_{12} are prescribed to vanish identically, while the in-plane shear strain increases gradually at constant strain rate. The critical directions giving rise to localized failure will be studied by means of a non-associated parabolic Drucker–Prager plasticity formulation. Thereby, the influence of lateral confinement is increased gradually by increasing the ratio of compressive to tensile strength $f_c : f_t$. This ratio directly affects the value of the friction coefficient α_F^{mac} whereas, the parameter α_Q^{mac} is kept constant at zero, thus introducing a plastic potential of von Mises type.

Table 1 summarizes the resulting critical failure angle Θ^{crit} for different Poisson's ratios and strength ratios $f_c : f_t$. The critical failure angle ranges from 0° to 45°, thus characterizing a pure mode I type failure as well as mixed failure modes. As expected, the critical failure angle decreases with an increase of lateral confinement which is caused by increasing the mismatch of the compressive to tensile strength. Moreover, the influence of lateral confinement increases for larger values of Poisson's ratio.

Table 1
Critical failure angle Θ^{crit} – simple shear problem

$f_c : f_t$	$\nu = 0.000$	$\nu = 0.125$	$\nu = 0.250$	$\nu = 0.375$	$\nu = 0.499$
1:1	45.00°	45.00°	45.00°	45.00°	45.00°
3:1	35.26°	33.99°	32.69°	31.36°	30.01°
5:1	29.45°	27.24°	24.90°	22.38°	19.64°
8:1	22.20°	18.26°	13.37°	5.39°	0.00°
12:1	11.78°	0.00°	0.00°	0.00°	0.00°

Figs. 5–7 show the result of the corresponding geometric localization analysis on the basis of a simulation with Poisson's ratio of $\nu = 0.2$. The first figure of the series is based on a compressive to tensile strength ratio of one, $f_c : f_t = 1 : 1$. This choice corresponds to a vanishing friction coefficient, $\alpha_F^{mac} = 0.0$, thus representing the classical yield function of von Mises type. For this analysis, two critical directions can

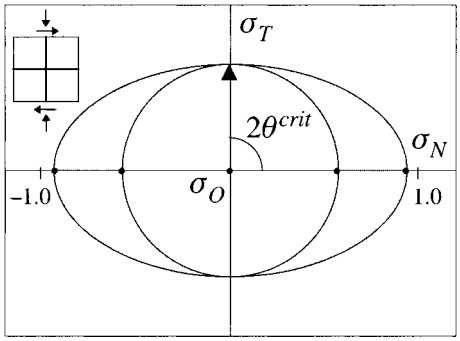

Fig. 5. Geometric localization analysis – $f_c : f_t = 1 : 1$.

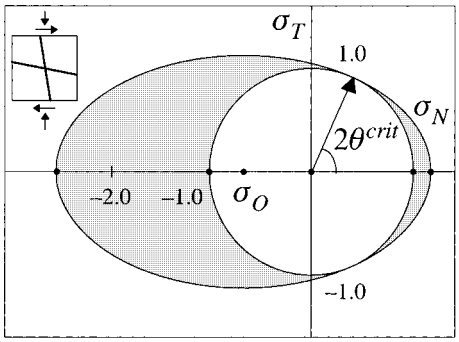

Fig. 6. Geometric localization analysis – $f_c : f_t = 3 : 1$.

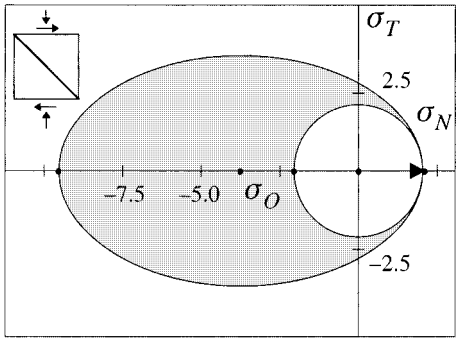

Fig. 7. Geometric localization analysis – $f_c : f_t = 12 : 1$.

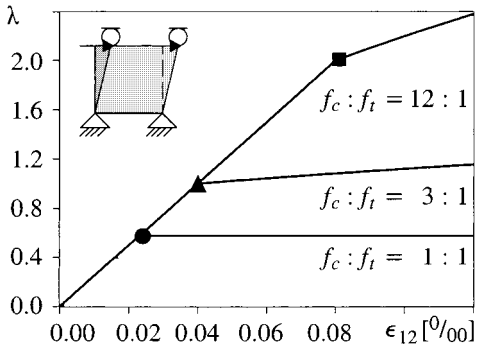

Fig. 8. Load factor vs. shear strains – $f_c : f_t = 1 : 1$, $3 : 1$ and $12 : 1$.

be found under $\Theta^{\text{crit}} = 45°$ and $\Theta^{\text{crit}} = 135°$ indicating a pure shear failure. This typical failure mode for pressure insensitive materials is characteristic for the well-known phenomenon of Lüders band formation in metals.

Fig. 6 depicts the result of a localization analysis for which the compressive strength is assumed to be three times larger than the tensile strength, $f_c : f_t = 3 : 1$. The corresponding friction coefficient of $\alpha_F^{\text{mac}} = 0.6667$ induces a relatively low confinement. Again, two critical directions can be found. However, they have rotated slightly towards the direction of maximum principal stress. The corresponding critical failure angles of $\Theta^{\text{crit}} = 33.211°$ and $\Theta^{\text{crit}} = 146.789°$ indicate a mixed shear compression failure.

Finally, the compressive strength is assumed to be 12 times larger than the tensile strength, $f_c : f_t = 12 : 1$, thus introducing a high confinement. The related friction coefficient takes a value of $\alpha_F^{\text{mac}} = 3.6667$, which corresponds to the one of cementitious materials like concrete. For this class of materials with a relatively large mismatch between compressive and tensile strength, a purely brittle failure mode can be observed. Fig. 7 illustrates the classical mode I failure for which the critical direction corresponds to the direction of maximum principal stress at $\Theta^{\text{crit}} = 0°$.

In addition to the analytical localization analysis, a numerical localization study on the material point level has been performed. Therefore, the rate equations of elasto-plasticity of Section 2 have to be discretized in time. An implicit Euler backward scheme in combination with a classical two-step predictor corrector algorithm is applied in order to perform the time integration. In this specific case, the corrector is based on a radial return since the plastic flow is assumed to be purely deviatoric. Fig. 8 depicts the resulting load factor versus shear strain curves of the three different analyses. The marked points of the corresponding curves indicate the onset of localization which coincides with the initiation of plastic yielding in all three cases. Obviously, due to the non-associated nature of the underlying plasticity formulation, localization may occur, or in other terms a spatial discontinuity may form in the hardening regime before a limit point has been reached.

5. Microplane-based elasto-plasticity

In this section, a microplane-based plasticity model is introduced, which is able to account for anisotropy in a natural fashion. Its basic features are borrowed from the kinematically constrained microplane damage models first presented by Bažant and Gambarova (1984), Bažant and Prat (1988) and Carol et al. (1992). The application to elasto-plasticity was discussed by Carol and Bažant (1997). In contrast to the existing microplane models based on the introduction of three different uncoupled strain components, we will restrict ourselves to a formulation which can be expressed exclusively in terms of the volumetric and the

tangential strains and stresses on the microplane. For this specific choice, which can be considered as a special case of the existing microplane formulations, the normal component on the microplane results exclusively from the volumetric projection. Note, that this specific microplane formulation does not imply, that the macroscopic strains are purely volumetric. Consequently, the normal deviatoric strains, which are considered in previous microplane formulations, do not necessarily have to vanish. However, it is assumed that the deviatoric strains do not contribute to the free energy on the microplane level. Motivated by the macroscopic plasticity formulation, we will introduce one single yield function on each microplane in order to account for the constitutive coupling between normal and tangential stress components.

5.1. Kinematic constraint

In accordance with the original microplane formulations, the model presented herein is based on the kinematic constraint. Accordingly, the individual strain components of one material plane, the scalar-valued volumetric strain ϵ_{V} and the tangential strain vector $\boldsymbol{\epsilon}_{\mathrm{T}}$, can be expressed as projections of the overall strain tensor $\boldsymbol{\epsilon}$

$$\begin{aligned} \epsilon_{\mathrm{V}} &= \boldsymbol{V} : \boldsymbol{\epsilon}, \\ \boldsymbol{\epsilon}_{\mathrm{T}} &= \boldsymbol{T} : \boldsymbol{\epsilon} \end{aligned} \tag{45}$$

with the volumetric and the tangential projection tensor $\boldsymbol{V}$ and $\boldsymbol{T}$, which are of second and third order, respectively.

$$\begin{aligned} \boldsymbol{V} &= \tfrac{1}{3}\mathbf{1}, \\ \boldsymbol{T} &= \mathbf{n} \cdot \mathscr{I} - \boldsymbol{n} \otimes \boldsymbol{n} \otimes \boldsymbol{n}. \end{aligned} \tag{46}$$

As illustrated in Fig. 9, the strain vector $\boldsymbol{t}_{\epsilon}$ of the corresponding plane can be understood as the sum of the plane's normal $\boldsymbol{n}$ scaled by the volumetric strain and the tangential strain vector.

$$\boldsymbol{t}_{\epsilon} = \epsilon_{\mathrm{V}}\, \boldsymbol{n} + \boldsymbol{\epsilon}_{\mathrm{T}}. \tag{47}$$

5.2. Constitutive equations

The constitutive equations of the microplane-based plasticity model, can be introduced in analogy to the macroscopic plasticity formulation. They are based on the additive decomposition of the volumetric and the tangential strain component into elastic and plastic parts:

$$\begin{aligned} \epsilon_{\mathrm{V}} &= \epsilon_{\mathrm{V}}^{\mathrm{el}} + \epsilon_{\mathrm{V}}^{\mathrm{pl}}, \\ \boldsymbol{\epsilon}_{\mathrm{T}} &= \boldsymbol{\epsilon}_{\mathrm{T}}^{\mathrm{el}} + \boldsymbol{\epsilon}_{\mathrm{T}}^{\mathrm{pl}}. \end{aligned} \tag{48}$$

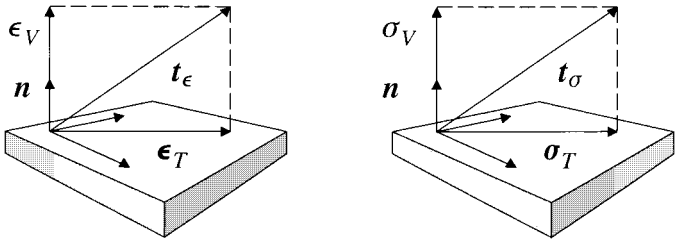

Fig. 9. Strain and stress components on microplane.

The free energy Ψ^{mic} related to one individual microplane can thus be introduced as a function of the total and the plastic strain components and an internal variable κ which accounts for the hardening behavior:

$$\Psi^{\mathrm{mic}} = \Psi^{\mathrm{mic}}(\epsilon_{\mathrm{V}}, \epsilon_{\mathrm{V}}^{\mathrm{pl}}, \boldsymbol{\epsilon}_{\mathrm{T}}, \boldsymbol{\epsilon}_{\mathrm{T}}^{\mathrm{pl}}, \kappa). \tag{49}$$

Consequently, the volumetric and the tangential stress components σ_{V} and $\boldsymbol{\sigma}_{\mathrm{T}}$ are given as the conjugate quantities to the corresponding strains such that

$$\begin{aligned} \sigma_{\mathrm{V}} &= \frac{\partial \Psi^{\mathrm{mic}}}{\partial \epsilon_{\mathrm{V}}^{\mathrm{el}}} \quad \text{and} \quad \dot{\sigma}_{\mathrm{V}} = \mathscr{E}_{\mathrm{V}}^{\mathrm{el}} \left[\dot{\epsilon}_{\mathrm{V}} - \dot{\epsilon}_{\mathrm{V}}^{\mathrm{pl}} \right], \\ \boldsymbol{\sigma}_{\mathrm{T}} &= \frac{\partial \Psi^{\mathrm{mic}}}{\partial \boldsymbol{\epsilon}_{\mathrm{T}}^{\mathrm{el}}} \quad \text{and} \quad \dot{\boldsymbol{\sigma}}_{\mathrm{T}} = \mathscr{E}_{\mathrm{T}}^{\mathrm{el}} \left[\dot{\boldsymbol{\epsilon}}_{\mathrm{T}} - \dot{\boldsymbol{\epsilon}}_{\mathrm{T}}^{\mathrm{pl}} \right], \end{aligned} \tag{50}$$

whereby $\mathscr{E}_{\mathrm{V}}^{\mathrm{el}}$ and $\mathscr{E}_{\mathrm{T}}^{\mathrm{el}}$ denote the volumetric and the tangential elastic microplane modulus, respectively. Moreover, the microplane-based yield stress Y_F^{mic} is introduced conjugate to the internal variable κ. The relation between the evolution of the yield stress and the rate of this internal variable defines the microplane-based softening modulus H, such that

$$Y_F^{\mathrm{mic}} = \frac{\partial \Psi^{\mathrm{mic}}}{\partial \kappa} \quad \text{and} \quad \dot{Y}_F^{\mathrm{mic}} = H\, \dot{\kappa}. \tag{51}$$

Similar to the macroscopic model, the elastic domain in the stress space is bounded by the yield function F^{mic}

$$F^{\mathrm{mic}}\left(\sigma_{\mathrm{V}}, \boldsymbol{\sigma}_{\mathrm{T}}, Y_F^{\mathrm{mic}}\right) \leqslant 0 \quad \text{with } \nu_{\mathrm{V}} := \frac{\partial F^{\mathrm{mic}}}{\partial \sigma_{\mathrm{V}}} \quad \text{and} \quad \boldsymbol{\nu}_{\mathrm{T}} := \frac{\partial F^{\mathrm{mic}}}{\partial \boldsymbol{\sigma}_{\mathrm{T}}}, \tag{52}$$

whereby ν_{V} and $\boldsymbol{\nu}_{\mathrm{T}}$ denote its normal in the volumetric and the tangential direction. Note, that in order to take into account a normal-tangential coupling which is neglected in the original microplane models, a single-surface yield criterion has been introduced on the microplane level. The evolution of the plastic strain components ϵ_{V} and $\boldsymbol{\epsilon}_{\mathrm{T}}$ is determined by the volumetric and the tangential flow rule

$$\begin{aligned} \dot{\epsilon}_{\mathrm{V}}^{\mathrm{pl}} &= \dot{\gamma}\, \mu_{\mathrm{V}} \quad \text{with } \mu_{\mathrm{V}} := \frac{\partial Q^{\mathrm{mic}}}{\partial \sigma_{\mathrm{V}}}, \\ \dot{\boldsymbol{\epsilon}}_{\mathrm{T}}^{\mathrm{pl}} &= \dot{\gamma}\, \boldsymbol{\mu}_{\mathrm{T}} \quad \text{with } \boldsymbol{\mu}_{\mathrm{T}} := \frac{\partial Q^{\mathrm{mic}}}{\partial \boldsymbol{\sigma}_{\mathrm{T}}} \end{aligned} \tag{53}$$

with μ_{V} and $\boldsymbol{\mu}_{\mathrm{T}}$ denoting the flow directions which can be understood as normals to a plastic potential Q^{mic}. An associated flow rule is characterized through a plastic potential, which is identical to the yield function, such that $F^{\mathrm{mic}} = Q^{\mathrm{mic}}$. The Kuhn–Tucker conditions

$$F^{\mathrm{mic}} \leqslant 0, \;\; \dot{\gamma} \geqslant 0, \;\; F^{\mathrm{mic}}\, \dot{\gamma} = 0 \tag{54}$$

and the consistency condition

$$\dot{F}^{\mathrm{mic}}\, \dot{\gamma} = 0 \tag{55}$$

govern the loading–unloading process. Furthermore, the evaluation of the consistency condition yields the definition of the plastic multiplier γ of the following form:

$$\dot{\gamma} = \frac{1}{h} \left[\nu_{\mathrm{V}}\, \mathscr{E}_{\mathrm{V}}^{\mathrm{el}}\, \boldsymbol{V} + \boldsymbol{\nu}_{\mathrm{T}}\, \mathscr{E}_{\mathrm{T}}^{\mathrm{el}} \cdot \boldsymbol{T} \right] : \dot{\boldsymbol{\epsilon}} \tag{56}$$

with $h = H + \nu_{\mathrm{V}}\, \mathscr{E}_{\mathrm{V}}^{\mathrm{el}}\, \mu_{\mathrm{V}} + \boldsymbol{\nu}_{\mathrm{T}}\, \mathscr{E}_{\mathrm{T}}^{\mathrm{el}} \cdot \boldsymbol{\mu}_{\mathrm{T}}$.

5.3. Homogenization

In order to relate the response of all microplanes in space to the macroscopic response on the material point level, we will make use of the following fundamental assumption according to Carol et al. (2000):

$$\Psi^{\mathrm{mac}} = \frac{3}{4\pi} \int_{\Omega} \Psi^{\mathrm{mic}} \, \mathrm{d}\Omega. \tag{57}$$

It states, that the free energy of a material point can be understood as the integral of all microplane-based free energies integrated over the entire solid angle Ω. Following the traditional line of deriving constitutive formulations, the overall stresses tensor is derived from the evaluation of the Clausius–Duhem inequality. It is thus defined as the thermodynamically conjugate quantity to the macroscopic strains. A combination of the above equation with Eq. (57) yields the definition of the macroscopic stress tensor,

$$\boldsymbol{\sigma} = \frac{\partial \Psi^{\mathrm{mac}}}{\partial \boldsymbol{\epsilon}^{\mathrm{el}}} = \frac{3}{4\pi} \int_{\Omega} \left[\boldsymbol{V} \, \frac{\partial \Psi^{\mathrm{mic}}}{\partial \epsilon_{\mathrm{V}}^{\mathrm{el}}} + \boldsymbol{T}^{\mathrm{T}} \cdot \frac{\partial \Psi^{\mathrm{mic}}}{\partial \boldsymbol{\epsilon}_{\mathrm{T}}^{\mathrm{el}}} \right] \mathrm{d}\Omega \tag{58}$$

which may be expressed in terms of the microplane stress components defined through Eq. (50) weighted by the individual projection tensors.

$$\boldsymbol{\sigma} = \frac{3}{4\pi} \int_{\Omega} \left[\boldsymbol{V} \, \sigma_{\mathrm{V}} + \boldsymbol{T}^{\mathrm{T}} \cdot \boldsymbol{\sigma}_{\mathrm{T}} \right] \mathrm{d}\Omega. \tag{59}$$

Eq. (59) may be understood as the symmetric part of the dyadic products of all traction vectors $\boldsymbol{t}_{\sigma}$ with the corresponding plane's normal integrated over the solid angle

$$\boldsymbol{\sigma} = \frac{3}{4\pi} \int_{\Omega} [\boldsymbol{t}_{\sigma} \otimes \boldsymbol{n}]^{\mathrm{sym}} \, \mathrm{d}\Omega \quad \text{with } \boldsymbol{t}_{\sigma} = \sigma_{\mathrm{V}} \, \boldsymbol{n} + \boldsymbol{\sigma}_{\mathrm{T}}, \tag{60}$$

whereby the definition of the traction vector is illustrated in Fig. 9. The macroscopic tangent operator relating the macroscopic stresses and strains can be derived in an analogous form:

$$\mathscr{E}^{\mathrm{ep}} = \frac{\mathrm{d}\boldsymbol{\sigma}}{\mathrm{d}\boldsymbol{\epsilon}} = \frac{3}{4\pi} \int_{\Omega} \left[\boldsymbol{V} \otimes \frac{\mathrm{d}\boldsymbol{\sigma}}{\mathrm{d}\epsilon_{\mathrm{V}}} + \boldsymbol{T}^{\mathrm{T}} \cdot \frac{\mathrm{d}\boldsymbol{\sigma}}{\mathrm{d}\boldsymbol{\epsilon}_{\mathrm{T}}} \right] \mathrm{d}\Omega. \tag{61}$$

Similar to the overall stress tensor, it can be expressed exclusively in terms of the quantities on the microplanes weighted by the individual projection tensors:

$$\mathscr{E}^{\mathrm{ep}} = \mathscr{E}^{\mathrm{el}} - \frac{3}{4\pi} \int_{\Omega} \frac{1}{h} \left[\mathscr{E}_{\mathrm{V}}^{\mathrm{el}} \, \boldsymbol{V} \, \mu_{\mathrm{V}} + \mathscr{E}_{\mathrm{T}}^{\mathrm{el}} \, \boldsymbol{T}^{\mathrm{T}} \cdot \boldsymbol{\mu}_{\mathrm{T}} \right] \otimes \left[\nu_{\mathrm{V}} \, \boldsymbol{V} \, \mathscr{E}_{\mathrm{V}}^{\mathrm{el}} + \boldsymbol{\nu}_{\mathrm{T}} \cdot \, \boldsymbol{T} \, \mathscr{E}_{\mathrm{T}}^{\mathrm{el}} \right] \mathrm{d}\Omega. \tag{62}$$

In analogy to the macroscopic formulation of plasticity where the pressure sensitivity of the plastic flow rule is responsible for shear dilatancy, a sufficient microplane condition is obtained for coupling volumetric and tangential components when each microplane satisfies the inequality

$$\mathbf{1} : \left[\mathscr{E}_{\mathrm{V}}^{\mathrm{el}} \, \boldsymbol{V} \, \mu_{\mathrm{V}} + \mathscr{E}_{\mathrm{T}}^{\mathrm{el}} \, \boldsymbol{T}^{\mathrm{T}} \cdot \boldsymbol{\mu}_{\mathrm{T}} \right] = \mathbf{1} : \left[\mathscr{E}_{\mathrm{V}}^{\mathrm{el}} \, \mathbf{V} \, \mu_{\mathrm{V}} \right] > 0 \quad \text{or} \quad \alpha_{Q}^{\mathrm{mic}} > 0. \tag{63}$$

This equivalent to say that $\alpha_{Q}^{\mathrm{mic}} > 0$ on each microplane, assures coupling and captures the Reynolds effect. In this context it is important to note that the volumetric component is the same on all microplanes and does not depend on the orientation of a specific microplane. In fact, it is this particular feature which introduces a common volumetric contribution in the yield condition and thus interaction among the plastic action on each microplane.

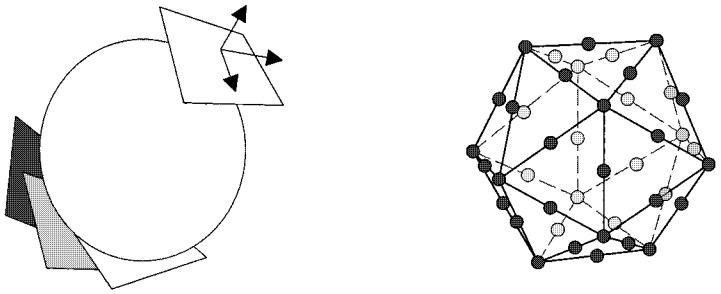

Fig. 10. Discretization of solid angle with 42 integration points.

5.4. Discretization of solid angle

In the previous section, the overall quantities have been defined through integral expressions. The analytical evaluation of these integrals can be very difficult or even impossible in the general anisotropic case. Therefore, Bažant and Oh (1985, 1986) have proposed to apply a numerical integration technique, whereby the integral over the solid angle is replaced by a sum of the corresponding term evaluated at discrete integration points:

$$\frac{3}{4\pi}\int_{\Omega}(\bullet)\,\mathrm{d}\Omega \approx \sum_{I=1}^{n_{mp}}(\bullet)^{I} w^{I}. \tag{64}$$

Herein, w^I is the weighting coefficient of the I's point, whereas n_{mp} denotes the total number of integration points. Within this study, an integration with $n_{mp} = 42$ integration points has been applied. The geometry of these points, which goes back to Stroud (1971), is depicted in Fig. 10. The numerically approximated macroscopic stresses tensor thus takes the following form

$$\boldsymbol{\sigma} \approx \sum_{I=1}^{n_{mp}} \left[\sigma_{\mathrm{V}}^{I}\,\boldsymbol{V}^{I} + \boldsymbol{\sigma}_{\mathrm{T}}^{I}\cdot\boldsymbol{T}^{I}\right] w^{I}, \tag{65}$$

while the macroscopic tangent operator can be approximated as follows:

$$\mathscr{E}^{\mathrm{ep}} \approx \mathscr{E}^{\mathrm{el}} - \sum_{I=1}^{n_{mp}} \frac{1}{h^{\mathrm{mic}\,I}}\left[\mathscr{E}_{\mathrm{V}}^{\mathrm{el}}\,\boldsymbol{V}^{I}\,\mu_{\mathrm{V}}^{I} + \mathscr{E}_{\mathrm{T}}^{\mathrm{el}}\,\boldsymbol{T}^{\mathrm{T}\,I}\cdot\boldsymbol{\mu}^{I}\right]\otimes\left[v_{\mathrm{V}}^{I}\,\boldsymbol{V}^{I}\,\mathscr{E}_{\mathrm{V}}^{\mathrm{el}} + \boldsymbol{v}_{\mathrm{T}}^{I}\cdot\boldsymbol{T}^{I}\,\mathscr{E}_{\mathrm{T}}^{\mathrm{el}}\right] w^{I}. \tag{66}$$

6. Microplane-based failure analysis

6.1. Diffuse failure–loss of uniqueness

According to the results of Section 3.1, the loss of uniqueness on the material point level corresponds to the singular behavior of the elasto-plastic tangent operator which takes the following form for the microplane-based plasticity model:

$$\det \mathscr{E}^{\mathrm{ep}} \stackrel{!}{=} 0 \quad \text{with } \mathscr{E}^{\mathrm{ep}} = \mathscr{E}^{\mathrm{el}} - \frac{3}{4\pi}\int_{\Omega}\frac{\overline{\boldsymbol{\mu}}\otimes\overline{\boldsymbol{v}}}{h}\mathrm{d}\Omega. \tag{67}$$

Note that herein, the following abbreviations have been introduced:

$$\begin{aligned}\overline{\boldsymbol{\mu}} &:= \mathscr{E}_{\mathrm{V}}^{\mathrm{el}} \boldsymbol{V} \mu_{\mathrm{V}} + \mathscr{E}_{\mathrm{T}}^{\mathrm{el}} \boldsymbol{T}^{\mathrm{T}} \cdot \boldsymbol{\mu}_{\mathrm{T}}, \\ \overline{\boldsymbol{v}} &:= v_{\mathrm{V}} \boldsymbol{V} \mathscr{E}_{\mathrm{V}}^{\mathrm{el}} + \boldsymbol{v}_{\mathrm{T}} \cdot \boldsymbol{T} \mathscr{E}_{\mathrm{T}}^{\mathrm{el}}.\end{aligned} \tag{68}$$

The solution of the corresponding generalized eigenvalue problem $\det[[\boldsymbol{\mathscr{E}}^{\mathrm{el}}]^{-1} : \boldsymbol{\mathscr{E}}^{\mathrm{ep}}]$ requires a pre-conditioning with the inverse of the elasticity tensor:

$$\left[\boldsymbol{\mathscr{E}}^{\mathrm{el}}\right]^{-1} : \boldsymbol{\mathscr{E}}^{\mathrm{ep}} = \boldsymbol{\mathscr{I}} - \left[\boldsymbol{\mathscr{E}}^{\mathrm{el}}\right]^{-1} : \frac{3}{4\pi} \int_{\Omega} \frac{\overline{\boldsymbol{\mu}} \otimes \overline{\boldsymbol{v}}}{h} \mathrm{d}\Omega. \tag{69}$$

In contrast to the macroscopic elasto-plastic tangent operator, the update structure of the microplane-based tangent moduli is of multiple rank. Consequently, the related measure of material integrity $D_{\mathscr{E}}$ which is defined in terms of the smallest eigenvalue of the generalized eigenvalue problem $\lambda_{\min}[[\boldsymbol{\mathscr{E}}^{\mathrm{el}}]^{-1} : \boldsymbol{\mathscr{E}}^{\mathrm{ep}}] = 1 - D_{\mathscr{E}}$ can only be calculated numerically.

6.2. Localized failure–loss of ellipticity

In Section 3.2, we have introduced the localization condition for the macroscopic plasticity model. Its microplane-based counterpart can be expressed as follows:

$$\det \boldsymbol{q}^{\mathrm{ep}} \stackrel{!}{=} 0 \quad \text{with } \boldsymbol{q}^{\mathrm{ep}} = \boldsymbol{q}^{\mathrm{el}} - \frac{3}{4\pi} \int_{\Omega} \frac{\boldsymbol{e}_{\mu} \otimes \boldsymbol{e}_{v}}{h} \mathrm{d}\Omega, \tag{70}$$

whereby the following abbreviations for the update vectors $\boldsymbol{e}_{\mu}$ and $\boldsymbol{e}_{v}$ have been applied:

$$\begin{aligned}\boldsymbol{e}_{\mu} &:= \boldsymbol{n} \cdot \left[\mathscr{E}_{\mathrm{V}}^{\mathrm{el}} \boldsymbol{V} \mu_{\mathrm{V}} + \mathscr{E}_{\mathrm{T}}^{\mathrm{el}} \boldsymbol{T}^{\mathrm{T}} \cdot \boldsymbol{\mu}_{\mathrm{T}}\right], \\ \boldsymbol{e}_{v} &:= \left[v_{\mathrm{V}} \boldsymbol{V} \mathscr{E}_{\mathrm{V}}^{\mathrm{el}} + \boldsymbol{v}_{\mathrm{T}} \cdot \boldsymbol{T} \mathscr{E}_{\mathrm{T}}^{\mathrm{el}}\right] \cdot \boldsymbol{n}.\end{aligned} \tag{71}$$

The solution of the generalized eigenvalue problem $\det[[\boldsymbol{q}^{\mathrm{el}}]^{-1} \cdot \boldsymbol{q}^{\mathrm{ep}}] \stackrel{!}{=} 0$ involves pre-conditioning with the elastic acoustic tensor:

$$\left[\boldsymbol{q}^{\mathrm{el}}\right]^{-1} \cdot \boldsymbol{q}^{\mathrm{ep}} = \boldsymbol{1} - \left[\boldsymbol{q}^{\mathrm{el}}\right]^{-1} \cdot \frac{3}{4\pi} \int_{\Omega} \frac{\boldsymbol{e}_{\mu} \otimes \boldsymbol{e}_{v}}{h} \mathrm{d}\Omega. \tag{72}$$

However, it becomes obvious, that the related measure of localization integrity D_q resulting from the smallest eigenvalue

$$\lambda_{\min}\left[\left[\boldsymbol{q}^{\mathrm{el}}\right]^{-1} \cdot \boldsymbol{q}^{\mathrm{ep}}\right] = 1 - D_q \tag{73}$$

can be calculated only numerically because of the multiple rank-one update structure of the microplane-based acoustic tensor.

7. Example: non-associated Drucker–Prager plasticity

7.1. Specification of yield function and plastic potential

The current microplane formulations are all based on independent yield (failure) functions for each traction component resulting in a multi-surface plasticity (failure) formulation on each microplane. Within this study, we will introduce a single-surface yield function on each microplane which is motivated by the macroscopic Drucker–Prager formulation. The microplane-based analog on to the generalized formulation of Eq. (28) can thus be expressed as follows:

$$F^{\mathrm{mic}} = F^{\mathrm{mic}}(\sigma_{\mathrm{V}}, \boldsymbol{\sigma}_{\mathrm{T}}, Y_F^{\mathrm{mic}}) = \tfrac{1}{2}\left[\boldsymbol{\sigma}_{\mathrm{T}} \cdot \boldsymbol{\sigma}_{\mathrm{T}}\right]^m - z\left[c\, \alpha_F^{\mathrm{mic}}\, \sigma_{\mathrm{V}} - Y_F^{\mathrm{mic}}\right]^n, \tag{74}$$

whereby the original two invariant formulation in terms of I_1 and J_2 has been modified into a formulation in terms of σ_V and $\boldsymbol{\sigma}_T$. Again, for the specific choice of $m = 1$, $z = -1$, $c = 1$ and $n = 1$, the corresponding yield function represents a parabola in the $\{\sigma_V, \boldsymbol{\sigma}_T\}$-space:

$$\begin{aligned} F^{mic} &= F^{mic}(\sigma_V, \boldsymbol{\sigma}_T, Y_F^{mic}) = \tfrac{1}{2}\,\boldsymbol{\sigma}_T \cdot \boldsymbol{\sigma}_T + \alpha_F^{mic}\,\sigma_V - Y_F^{mic}, \\ Q^{mic} &= Q^{mic}(\sigma_V, \boldsymbol{\sigma}_T, Y_Q^{mic}) = \tfrac{1}{2}\,\boldsymbol{\sigma}_T \cdot \boldsymbol{\sigma}_T + \alpha_Q^{mic}\,\sigma_V - Y_Q^{mic}. \end{aligned} \tag{75}$$

The corresponding plastic potential has been chosen in a similar fashion in analogy to the macroscopic plasticity formulation of Section 4.1.

7.2. Adjustment of material parameters

In this section, relations between the microplane-based parameters and well-known macroscopic material parameters will be pointed out. We will start by comparing the microplane-based elastic parameters to the macroscopic bulk and shear modulus. The analysis is motivated by a comparison of the coefficients of both elasticity tensors. The fourth order elasticity tensor can be derived as a special case of Eq. (62).

$$\mathscr{E}^{el} = \frac{3}{4\pi} \int_\Omega \mathscr{E}_V^{el}\, \boldsymbol{V} \otimes \boldsymbol{V} + \mathscr{E}_T^{el}\, \boldsymbol{T}^T \cdot \boldsymbol{T}\, d\Omega. \tag{76}$$

For isotropic elasticity, the elastic microplane moduli $\mathscr{E}_V^{el}$ and $\mathscr{E}_T^{el}$ are identical for each plane and can thus be written in front of the integral. The remaining integral expressions can be solved analytically by making use of the below integration properties according to Lubarda and Krajcinovic (1993).

$$\begin{aligned} &\int_\Omega d\Omega = 4\pi, \\ &\int_\Omega \boldsymbol{n} \otimes \boldsymbol{n}\, d\Omega = \frac{4\pi}{3}\,\mathbf{1}, \\ &\int_\Omega \boldsymbol{n} \otimes \boldsymbol{n} \otimes \boldsymbol{n} \otimes \boldsymbol{n}\, d\Omega = \frac{4\pi}{3}\left[\mathscr{I}^{vol} + \frac{2}{5}\mathscr{I}^{dev}\right] \end{aligned} \tag{77}$$

which lead to the following integration formulae for the projection tensors, compare also Bažant and Prat (1988).

$$\begin{aligned} &\frac{3}{4\pi} \int_\Omega \boldsymbol{V} \otimes \boldsymbol{V}\, d\Omega = \mathscr{I}^{vol}, \\ &\frac{3}{4\pi} \int_\Omega \boldsymbol{T}^T \cdot \boldsymbol{T}\, d\Omega = \frac{3}{5}\,\mathscr{I}^{dev}. \end{aligned} \tag{78}$$

A comparison of the microplane-based elasticity tensor with the elasticity tensor of Hooke's law

$$\begin{aligned} \mathscr{E}^{el} &= \mathscr{E}_V^{el}\mathscr{I}^{vol} + \tfrac{3}{5}\,\mathscr{E}_T^{el}\mathscr{I}^{dev}, \\ \mathscr{E}^{el} &= 3\,K\mathscr{I}^{vol} + 2\,G\mathscr{I}^{dev} \end{aligned} \tag{79}$$

yields a direct relation between the volumetric and the microplane-based elastic moduli and the macroscopic bulk modulus K and shear modulus G.

$$\mathscr{E}_V^{el} = 3\,K \quad \text{and} \quad \mathscr{E}_T^{el} = \tfrac{10}{3}\,G. \tag{80}$$

Moreover, due to the assumption of a kinematic constraint, relations between the invariants of the strain tensor and the microplane strain components can be set up. It turns out that the first invariant of macroscopic strain tensor can be expressed exclusively in terms of the volumetric microplane strains,

$$I_1 = \boldsymbol{\epsilon} : \mathbf{1} = \frac{3}{4\pi} \int_\Omega \epsilon_V \, d\Omega \tag{81}$$

while the second invariant of macroscopic strain deviator is given in terms of the tangential strain vectors.

$$J_2 = \frac{1}{2} \boldsymbol{\epsilon}^{dev} : \boldsymbol{\epsilon}^{dev} = \frac{3}{4\pi} \int_\Omega \frac{3}{10} \boldsymbol{\epsilon}_T \cdot \boldsymbol{\epsilon}_T \, d\Omega. \tag{82}$$

Note, that in the elastic regime, these relations between the invariants and the microplane components equally hold for the macroscopic stress invariants and microplane-based stress components. For the stress variables, however, these relations are only valid until the first microplane starts yielding:

$$I_1 \approx \frac{3}{4\pi} \int_\Omega \sigma_V \, d\Omega \quad \text{and} \quad J_2 \approx \frac{3}{4\pi} \int_\Omega \frac{3}{10} \boldsymbol{\sigma}_T \cdot \boldsymbol{\sigma}_T \, d\Omega. \tag{83}$$

Nevertheless, we will make use of the above expressions in order to quantify the relation between the microplane-based friction coefficient and microplane yield stress to their macroscopic counterparts. The subsequent example of the simple shear test will show that the results in the purely elastic as well as in the fully plastified state are indeed comparable. The approximated stress invariants (83) will be combined with the macroscopic parabolic Drucker–Prager yield function given in Eq. (29) and compared to the microplane-based yield function (75).

$$F^{mac} \approx \frac{3}{4\pi} \int_\Omega \left[\frac{3}{10} \boldsymbol{\sigma}_T \cdot \boldsymbol{\sigma}_T + \frac{f_c - f_t}{3} \sigma_V - \frac{1}{3} \frac{f_c f_t}{3} \right] d\Omega, \tag{84a}$$

$$F^{mic} = \frac{1}{2} \boldsymbol{\sigma}_T \cdot \boldsymbol{\sigma}_T + \alpha_F^{mic} \sigma_V - Y_F^{mic}. \tag{84b}$$

A comparison of the coefficients of the macroscopic expression (84a) multiplied by 5/3 with the microplane-based yield function (84b) yields approximations for the microplane friction coefficient α_F^{mic} and the microplane yield stress Y_F^{mic}:

$$\alpha_F^{mic} \approx \frac{5}{3} \frac{f_t - f_c}{3} \quad \text{and} \quad Y_F^{mic} \approx \frac{5}{9} \frac{f_c f_t}{3}. \tag{85}$$

Remarkably, due to the specific structure of the parabolic yield surface, the microplane friction coefficient takes five-third of its macroscopic value, whereas, the microplane yield stress is only approximately five-ninth of its macroscopic counterpart.

7.3. Model problem of simple shear

In the following, the results of a numerical localization analysis based on the parabolic Drucker–Prager based microplane plasticity model will be presented and compared to the corresponding results of the macroscopic localization analysis of Section 4.3. In analogy to the algorithmic realization of the macroscopic model, an implicit Euler backward algorithm is a combination with the classical predictor corrector scheme that is applied to discretize the underlying rate equations in the time domain. The Reynolds effect is again studied with the help of the simple shear problem by varying the friction coefficient α_F^{mic} while the parameter $\alpha_Q^{mic} = 0$ is kept constant at zero. Fig. 11 summarizes the results of the numerical localization analysis on the basis of a simulation with Poisson's ratio of $\nu = 0.2$. Thereby, again the three different strength ratios are used: $f_c : f_t = 1 : 1$ leads to an associated von Mises type plasticity formulation on each microplane, $f_c : f_t = 3 : 1$, introduce a low level of confinement and $f_c : f_t = 12 : 1$ a high confinement level characteristic for concrete materials. Each diagram depicts the values of the normalized acoustic tensor $\det \boldsymbol{q}^{ep} / \det \boldsymbol{q}^{el}$ for the different directions in space in cylindrical coordinates.

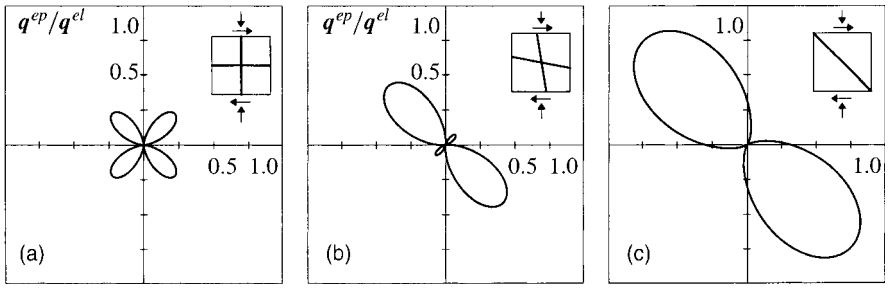

Fig. 11. Numerical localization analysis – $f_c : f_t = 1 : 1$, $3 : 1$ and $12 : 1$.

Obviously, for the associated plasticity formulation depicted in Fig. 11(a), with $f_c : f_t = 1 : 1$ and thus $\alpha_F^{mic} = 0.0$ the result is similar to the macroscopic plasticity formulation, (Fig. 7). It is characterized by a shear failure mode with two critical directions under $\Theta^{crit} = 45°$ and $\Theta^{crit} = 135°$. Fig. 11(b) shows the results of the low strength ratio with $f_c : f_t = 3 : 1$ corresponding to $\alpha_F^{mic} = 1.1111$. It is almost identical to the analytical localization analysis for the macroscopic plasticity model showing a mixed shear compression failure Fig. 6. The critical failure angles resulting from the numerical analysis take values of $\Theta^{crit} = 32.75°$ and $\Theta^{crit} = 147.25$ thus differing only slightly from the analytical results of $\Theta^{crit} = 33.211°$ and $\Theta^{crit} = 146.789°$. The last diagram of the series reflects the similar brittle failure mode as the macroscopic analysis of Fig. 7. It results from the analysis with $f_c : f_t = 12 : 1$ and $\alpha_F^{mic} = 6.1111$. Only one critical direction can be observed which corresponds to the direction of maximum principal stress. The critical failure angle of $\Theta^{crit} = 0°$ thus indicates a pure mode I failure.

Fig. 12 illustrates the load factor versus shear strain curves of the three analyses. Remarkably, the linear hardening on the microplane level results in a partially non-linear macroscopic response. The first mark of each curve corresponds to the situation, at which the first microplane starts yielding. Until the second mark is reached, a progressive onset of yielding takes places and all the other microplanes enter the plastic regime. As soon as the last microplane starts to plastify, the measure of localization integrity D_q reaches its critical value of one. This situation is indicated by the second mark in each curve. In contrast to the macroscopic plasticity model, the onset of localization no longer corresponds to the onset of plastic yielding. Localized failure is slightly delayed until plasticity has fully developed on all microplanes.

The results demonstrate, that under proportional loading, the microplane-based plasticity formulation shows the same characteristics as the macroscopic model provided that the related material parameters are

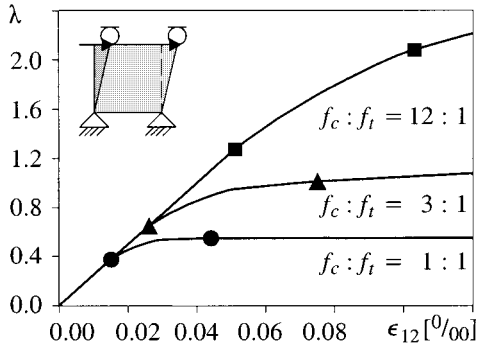

Fig. 12. Load factor vs. shear strains – $f_c : f_t = 1 : 1$, $3 : 1$ and $12 : 1$.

adjusted in an appropriate way (Fig. 8). It was shown that not only the principal features of both models are comparable, but also the two localization analysis yield remarkably similar results.

8. Summary and conclusions

On the macroscopic scale, the behavior of cohesive frictional materials was characterized through a generalized Drucker–Prager formulation of elasto-plasticity. The ensuing elasto-plastic tangent operator has the classical structure of rank-one updates, thus a closed form solution could be presented for the loss of uniqueness and the loss of ellipticity and illustrated at the example of simple shear.

The microplane concept served as the basis for a wide class of anisotropic constitutive formulations generalizing the classical notion of frictional sliding on characteristic planes of weaknesses. Thereby, the pointwise constitutive response was obtained through integration of non-linear material processes on each microplane over all possible orientations. In order to account for the characteristic behavior of cohesive frictional materials, a pressure-sensitive counterpart to the classical crystal plasticity formulation was introduced on each microplane along the lines of Drucker–Prager plasticity. Thereby, independent yield functions were formulated in terms of the volumetric and the tangential stress components on each microplane.

Since the structure of the microplane-based tangent operator is very complex, its analysis had to be restricted to numerical simulations of different failure scenarios. It was shown geometrically, how the critical failure mode introduced active plastic sliding on specific microplanes. Finally, the failure characteristics of the microplane model were compared with the analytical results of the generalized Drucker–Prager formulation with the model problem of simple shear.

To conclude, the failure study on the macrolevel of continuum plasticity and on the level of microplane plasticity showed comparable response behavior and localized failure modes in simple shear. Thereby, it was essential to incorporate an yield condition on each microplane which couples the tangential shear component with the volumetric stress.

Acknowledgements

The first and second author would like to acknowledge the support of the German National Science Foundation (DFG) through the graduate program 'Modellierung und Diskretisierungsmethoden für Kontinua und Strömungen' as well as through the research group 'Modellierung kohäsiver Reibungsmaterialien' under grant no. VE 163/4-1.4. The last author wishes to thank the Alexander von Humboldt Foundation for the research award and his host Professor Ekkehard Ramm at the University of Stuttgart. He also acknowledges the US National Science Foundation for the partial support of this effort under grant CMS-9634923 to the University of Colorado at Boulder.

References

Bažant, Z.P., Gambarova, P.G., 1984. Crack shear in concrete: crack band microplane model. J. Struct. Engng. ASCE 110, 2015–2036.

Bažant, Z.P., Oh, B.H., 1985. Microplane model for progressive fracture of concrete and rock. J. Engng. Mech. 111, 559–582.

Bažant, Z., Oh, B., 1986. Efficient numerical integration on the surface of a sphere. ZAMM 66, 37–49.

Bažant, Z.P., Prat, P., 1988. Microplane model for brittle plastic material: Part I – Theory, Part II – Verification. J. Engng. Mech. 114, 1672–1702.

Benallal, A., 1992. On localization phenomena in thermo-elasto-plasticity. Arch. Mech. 44, 15–29.

Benallal, A., Comi, C., 1996. Localization analysis via a geometrical method. Int. J. Solids Struct. 33, 99–119.

Carol, I., Prat, P., Bažant, Z.P., 1992. New explicit microplane model for concrete: theoretical aspects and numerical implementation. Int. J. Solids Struct. 29, 1173–1191.

Carol, I., Bažant, Z.P., 1997. Damage and plasticity in microplane theory. Int. J. Solids Struct. 34, 3807–3835.
Carol, I., Jirásek, M., Bažant, Z., 2000. A thermodynamically consistent approach to microplane theory. Part I & II: Free energy and consistent microplane stresses. Int. J. Solids Struct., in press.
Drucker, D.C., Prager, W., 1952. Soil mechanics and plastic analysis of limit design. Quart. Appl. Math. 10, 157–175.
Hadamard, J., 1903. Leçons sur la Propagation des Ondes. Librairie Scientifique A. Hermann et Fils, Paris.
Hill, R., 1958. A general theory of uniqueness and stability in elastic–plastic solids. J. Mech. Phys. Solids 6, 236–249.
Hill, R., 1962. Acceleration waves in solids. J. Mech. Phys. Solids 10, 1–16.
Iordache, M.M., Willam, K.J., 1998. Localized failure analysis in elasto-plastic Cosserat continua. Comp. Meth. Appl. Mech. Engng. 151, 559–586.
Iordache, M.M., Willam, K.J., 1997. Localized failure modes in cohesive frictional materials. Mech. Coh. Frict. Mat., submitted for publication.
Liebe, T., Willam, K., 1999. Localization results of generalized Drucker–Prager Elastoplasticity. Technical Note, University of Colorado at Boulder.
Lubarda, V.A., Krajcinovic, D., 1993. Damage tensors and the crack density distribution. Int. J. Solids Struct. 30, 2859–2877.
Mohr, O., 1882. Ueber die Darstellung des Spannungszustandes und des Deformationszustandes eines Körperelementes und über die Anwendung derselben in der Festigkeitslehre. Civilingenieur 28, 113–156.
Mohr, O., 1900a. Welche Umstände bedingen die Elastizitätsgrenze und den Bruch eines Materiales. Zeitschrift des Vereins Deutscher Ingenieure 46, 1524–1530.
Mohr, O., 1900b. Welche Umstände bedingen die Elastizitätsgrenze und den Bruch eines Materiales. Zeitschrift des Vereins Deutscher Ingenieure 46, 1572–1577.
Ottosen, N.S., Runesson, K., 1991. Properties of discontinuous bifurcation solutions in elasto-plasticity. Int. J. Solids Struct. 27, 401–421.
Pijaudier-Cabot, G., Benallal, A., 1993. Strain localization and bifurcation in a nonlocal continuum. Int. J. Solids Struct. 30, 1761–1775.
Reynolds, O., 1885. On the dilatancy of media composed of rigid particles in contact. Philos. Mag. J. Sci. 20, 469–481.
Rizzi, E., Carol, I., Willam, K.J., 1995. Localization analysis of elastic degradation with application to scalar damage. J. Engng. Mech. 121, 541–554.
Rudnicki, J.W., Rice, J.R., 1975. Conditions for the localization of deformation in pressure-sensitive dilatant materials. J. Mech. Phys. Solids 23, 371–394.
Stroud, A.H., 1971. Approximate calculation of multiple integrals. Prentice Hall, Englewood Cliffs, NJ.
Thomas, T.Y., 1961. Plastic Flow and Fracture of Solids. Academic Press, New York.
Willam, K., Hansen, E., Kang, H., 1999. Performance evaluation of damage and plasticity formulations for concrete. Proceedings of the US–Japan Seminar on Post-Peak Behavior of Reinforced Concrete Structures Subjected to Seismic Loads, ASCE Spec. Publ., New York.